Dual-Band Decoupling Between Extremely Closely Spaced PIFAs Based on *LC* Resonator

Zhongyao Cao, Le Chang, *Senior Member, IEEE*, Yue Li, *Senior Member, IEEE*, Kunpeng Wei, *Senior Member, IEEE*, and Zhijun Zhang, *Fellow, IEEE*

***Abstract*—In this article, we propose a simple scheme for dual-band antenna decoupling utilizing parallel *LC* resonators. By leveraging the common mode and differential mode (CM/DM) S-parameters, we provide a convenient method for distinguishing the coupling characteristics between the antennas. Based on this approach, we show that the dual-band PIFAs operating in the $TM_{0,0.5}$ and $TM_{1,0.5}$ modes exhibit electric and magnetic coupling (E/M coupling) in the respective frequency bands. The decoupling of these two bands can be achieved in a methodological way using the inductance of the parallel *LC* resonator below the resonant frequency and the capacitance above the resonant frequency. Decoupling for different frequency ratios can be readily adjusted by modifying the impedance characteristics of the *LC* resonator. By controlling the relative positions of the *LC* resonators, separate adjustments of decoupling in the two bands can be accomplished, thereby simplifying the decoupling process. To validate the effectiveness of the proposed method, a prototype is fabricated. The measured results demonstrated that the proposed scheme achieves effective isolation enhancement from 5 to 14 dB and 9 to 15 dB in two frequency bands, respectively. The proposed decoupling scheme offers a simple and efficient decoupling process with an easily realizable structure, making it a promising solution for future multi-input multi-output (MIMO) system designs.**

***Index Terms*—Antenna decoupling, common mode and differential mode (CM/DM) S-parameters, electric coupling (E coupling), *LC* resonator, magnetic coupling (M coupling).**

I. Introduction

HIGHER communication rate, smaller size, and integration are the continuous design aims of communication systems [1], [2], [3], [4]. Multi-input multi-output (MIMO) techniques have gained much attention due to the ability to improve channel capacity and reliability [5]. Due to the development of multiple communication protocols, multiband MIMO antennas with compact sizes are favored. However, the coupling of multiple operating bands becomes a key issue that limits the performance of the MIMO system.

In the past, there has been an amount of research work focusing on the decoupling of single-band MIMO antennas. Defected ground structures (DGSs) [6], [7] achieve decoupling by blocking the propagation of electromagnetic energy. By adding a neutralization line (NL) [8], [9], [10], metasurfaces [11], [12], parasitic branches or elements [13], [14], [15], new coupling paths are introduced for the cancellation of the original coupling. Recently, the common mode and differential mode (CM/DM) decoupling method and the active impedance matching method have been proposed, which provide a new perspective on the decoupling of two antennas and three antennas, respectively. Based on the CM/DM method and active impedance matching method, large numbers of designs with simple structures and guided design process for high isolation single-band operation have been proposed [16], [17], [18], [19].

The multiband operation of the antenna complicates the decoupling problem. Researchers have devoted themselves to extending the single-band decoupling technique to dual-band decoupling. DGS structures composed of two closely spaced quarter-wavelength slots [20], [21] and DGS structures with ground branches combined with slots [22], [23] were proposed for decoupling of the two operating bands. A single slot and ground branch both enable the decoupling of a single frequency band, but the inclusion of slots on the ground is undesired in many applications. Metasurface loaded above the antennas was proposed for dual-band decoupling by providing dual-band coupling [11], and controlling surface waves [24]. Decoupling branches [25], [26], [27] were added between the antennas for dual-band decoupling by introducing additional coupling. Introducing parasitic resonators between or beside the antennas is also an effective way for dual-band decoupling [28], [29], [30], [31], [32]. Decoupling techniques of loading parasitic resonators with two different resonant frequencies [28], [29], [30] or loading a single parasitic resonator with dual operating modes [31], [32] were proposed. Nevertheless, the added decoupling resonators require additional areas. In [33], [34], [35], and [36], by combining single-frequency decoupling structures such as metamaterials, decoupling resonators, and DGS, each of which decouples a single frequency band separately, the isolation of the two bands can be improved, respectively. The decoupling scheme, composed of two decoupling structures operating at two frequencies, has a simple design process but with a large size. A decoupling network provides a general way of multiband decoupling [37], [38], [39], but with a large size and complex design process. A dual-band decoupling design utilizing a single inductor for dual-band decoupling was proposed with a compact size and simple decoupling structure [38]. However, a single decoupling inductor cannot provide enough freedom in the decoupling of a dual-band antenna with different frequency ratios. Therefore, it remains a challenge to implement simple,

Received 28 December 2024; revised 10 June 2025; accepted 30 June 2025. Date of publication 16 July 2025; date of current version 30 October 2025. This work was supported in part by the National Natural Science Foundation of China under Contract 62271279. *(Corresponding author: Zhijun Zhang.)*

Zhongyao Cao, Yue Li, and Zhijun Zhang are with the Department of Electronic Engineering, Tsinghua University, Beijing 100084, China, and also with the Beijing National Research Center for Information Science and Technology, Tsinghua University, Beijing 100084, China (e-mail: zjzh@tsinghua.edu.cn).

Le Chang is with Shaanxi Key Laboratory of Deep Space Exploration Intelligent Information Technology, School of Information and Communications Engineering, Xi'an Jiaotong University, Xi'an 710049, China.

Kunpeng Wei is with Xiaomi Communications Company Ltd., Beijing 100085, China.

Digital Object Identifier 10.1109/TAP.2025.3587884

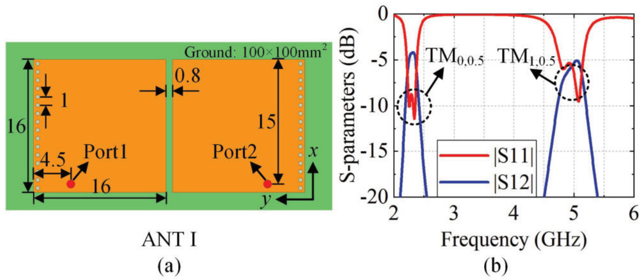

Fig. 1. (a) Configuration of Ant I composed of two closely spaced PIFAs without a decoupling *LC* resonator. (b) Simulated S-parameters of Ant I without decoupling the *LC* resonator.

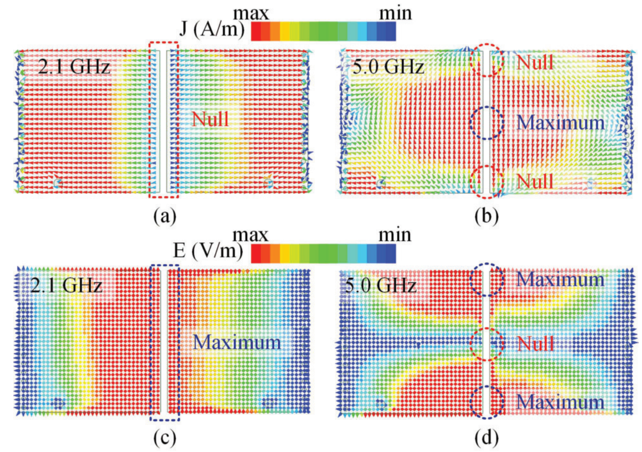

Fig. 2. Simulated current distribution of Ant I at (a) 2.1 GHz and (b) 5.0 GHz. Simulated electric field distribution of Ant I at (c) 2.1 GHz and (d) 5.0 GHz.

compact dual-band decoupling schemes with flexible and adjustable frequency ratios.

In this article, we propose a simple decoupling scheme based on *LC* resonators for dual-band PIFAs. With the help of CM/DM S-parameters, the electric coupling and the magnetic coupling (E/M coupling) between PIFAs can be discriminated. In turn, a clear design, physical intuition, and design guidance can be provided for the decoupling of *LC* resonators. The design process of decoupling is clear and simple. By changing the resonant frequency and the Q value of the *LC* resonator, the decoupling of PIFA antenna pairs with different frequency ratios can be performed. With the use of a lumped *LC* resonator, the isolation of two closely spaced PIFAs can be increased to have a good decoupling performance.

The main contribution of this work is summarized as follows.

1) By analyzing the S-parameters of the CM and DM modes, we propose to discriminate the coupling characteristics (E/M coupling) between the antenna pairs.
2) A methodological design process for dual-band decoupling utilizing *LC* resonators without iterative optimization is proposed.
3) Closely spaced dual-band PIFAs are proposed with the lumped decoupling structure integrated into the antenna pair, which provides a compact size.

The rest of this article is organized as follows. In Section II, the coupling characteristics between the antennas and the decoupling principle are analyzed. In Section III, the decoupling of dual-band antennas with different frequency ratios is presented and discussed. In Section IV, a simplified design process is provided. In Section V, the measured results are illustrated. Sections VI and VII present a comparison and summary of this work.

II. Principle of Decoupling Based on *LC* Resonator

A. Analysis of Coupling Characteristics

Fig. 1(a) shows the configuration of Ant I, which comprises two closely spaced PIFAs. The antenna pair is fabricated on a single FR-4 substrate ($\varepsilon_r = 4.4$, $\tan\delta = 0.02$) with dimensions of $100 \times 100 \times 1$ mm^3. The design is symmetrical along the central axes in both the *x*- and *y*-directions. Two feeding pins are applied to feed the PIFAs, with the feeding ports offset along the *x*-axis to enable the excitation of the $TM_{0,0.5}$ and $TM_{1,0.5}$ modes. As shown in Fig. 1(b), Ant I operates at frequency bands of 2.1 and 5.0 GHz. However, due to the minimal spacing between the antennas, significant mutual coupling is observed, resulting in the isolation of 4.2 and 5.1 dB at the lower and higher frequency bands, respectively.

The field distributions at the two operating bands are presented in Fig. 2. The coupling characteristics between the antennas are determined by the field distributions at their adjacent edges. As shown in Fig. 2(a) and (c), when the antenna operates in the $TM_{0,0.5}$ mode at the lower frequency band, the current at the adjacent edge is null while the electric field reaches its maximum. Consequently, the antennas exhibit E-coupling in the lower frequency band. In contrast, as displayed in Fig. 2(b), when the antennas operate in the $TM_{1,0.5}$ mode at the higher frequency band, the current distribution along the adjacent edge exhibits a maximum point and two nulls. Correspondingly, the electric field distribution shows two maximum points and one null point. On the edge, the coupling of current and electric field exists simultaneously. Based on the observed current and electric field distributions, it becomes challenging to identify whether the antennas exhibit E-coupling or M-coupling in the $TM_{1,0.5}$ mode. Additional analysis methods are required to clarify the coupling characteristics in this scenario.

CM/DM methods have been widely used in antenna decoupling [16], [17]. The decoupling problem of antenna pairs can be effectively analyzed through the impedance characteristics of the CM and DM. The passive S-parameters can be represented by CM and DM S-parameters as

$$S_{11} = S_{22} = \frac{S_{\mathrm{CM}} + S_{\mathrm{DM}}}{2} \quad (1)$$

$$S_{12} = S_{21} = \frac{S_{\mathrm{CM}} - S_{\mathrm{DM}}}{2}. \quad (2)$$

The mutual coupling and impedance matching can be achieved by matching the impedance of CM and DM simultaneously. Here, we analyze the coupling characteristics of the PIFA with the help of the CM and DM operating frequency. Fig. 3 presents the equivalent model of the two PIFAs with E/M coupling. The E-coupling is modeled as an equivalent capacitor C_0 between the two PIFAs, while the M-coupling is represented by an equivalent inductor L_0. For CM, the symmetry plane acts as a perfect magnetic conductor (PMC), rendering the equivalent capacitor C_0 and inductor L_0 open-circuited with no effect on the operating frequency of CMs.

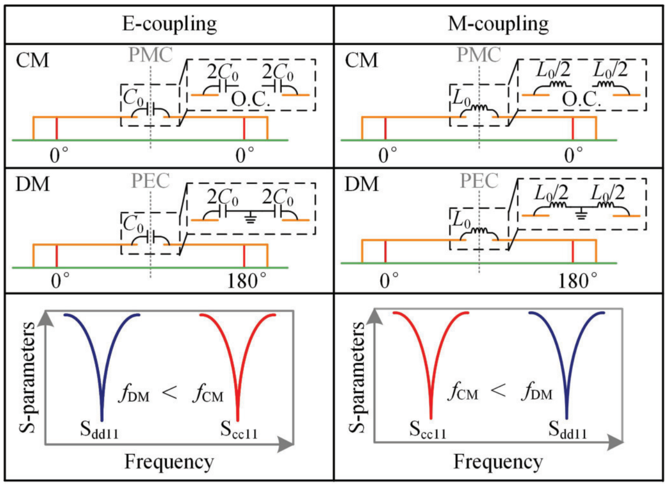

Fig. 3. Equivalent model of two PIFAs with E/M coupling and the corresponding CM/DM operating frequencies.

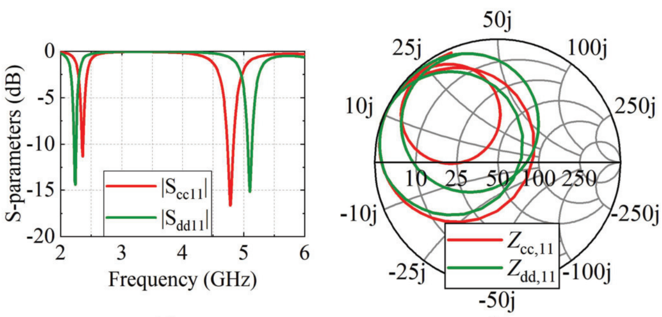

(a) (b)

Fig. 4. Simulated CM/DM S-parameters of the Ant I in (a) rectangular chart and (b) Smith chart.

Conversely, for DM, the symmetry plane behaves as a perfect electric conductor (PEC), resulting in the decomposition of the equivalent capacitor C_0 and inductor L_0 into two components connected to the ground. Capacitive loading [41] and inductive loading [42] on the PIFA are widely utilized to lower and raise the operating frequency, respectively. Therefore, different coupling characteristics lead to different frequency relationships between the CM and DM. Specifically, when the two PIFAs exhibit E-coupling, the operating frequency of DM is lower than that of CM. In contrast, for M-coupling, the operating frequency of DM is higher than that of CM. Hence, the coupling characteristics can be distinguished by the frequency relationship between CM and DM.

B. Decoupling Design

Fig. 4 shows the simulated CM/DM S-parameters. Based on the frequency relationship between CM and DM, it is determined that the two PIFAs are E-coupling in the lower frequency band and M-coupling in the higher frequency band. Consequently, in Fig. 2, the mutual coupling in the $TM_{1,0.5}$ mode is primarily dominated by the current distribution. Fig. 4(b) presents the CM/DM impedance on the Smith chart. For PIFAs, the impedance curves of CM/DM are both close to the matching point in the two modes of operation but exhibit a frequency offset. By adjusting the operating frequency of the DM mode, the CM/DM impedance can be brought together, thereby achieving decoupling.

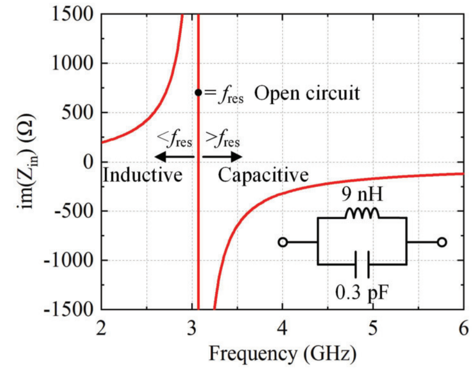

Fig. 5. Simulated impedance of the parallel LC resonator.

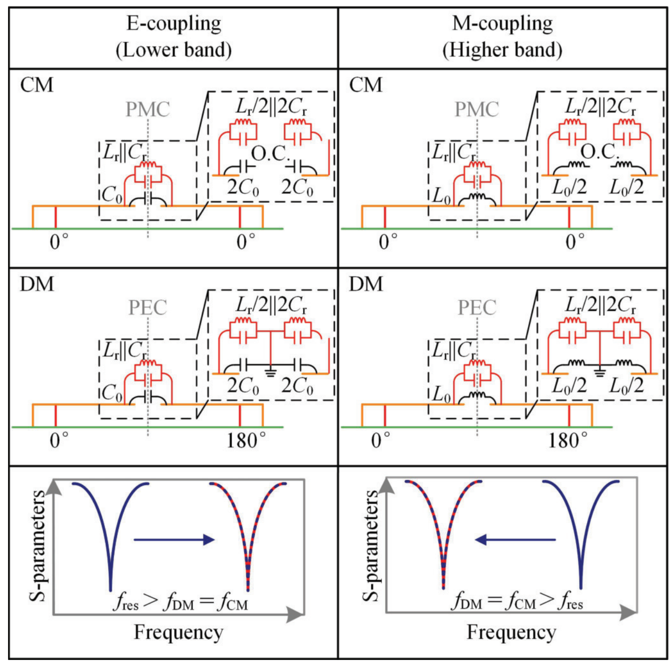

Fig. 6. Equivalent model of the PIFAs under CM/DM feeding with the addition of the LC resonator.

To eliminate the CM/DM frequency gap across both bands simultaneously, a parallel LC circuit is introduced between the PIFAs. As shown in Fig. 5, the resonant frequency f_{res} of the parallel LC resonator, consisting of a 6 nH inductor and a 0.3 pF capacitor, is 3.06 GHz. The LC resonator is capacitive above the resonant frequency and inductive below the resonant frequency. Fig. 6 illustrates the equivalent modal of the PIFAs with the LC resonator. Due to the existence of the PMC, the added LC resonator has no effect on the operating frequency of CM in both bands. However, for DM, the parallel LC resonator is equivalent to loading the PIFA with $L_r/2||2C_r$ connected to the ground. Since the resonator resonates between the two operating frequency bands of the PIFA, the LC resonator with the equivalent components C_0 and L_0 creates open circuits at both bands. Thus, the operating frequency of the DM can be tuned to the same as that of the CM in both modes at two frequency bands.

Fig. 7 illustrates the configuration of Ant I with the decoupling LC resonator and the corresponding S-parameters. Two LC resonators are loaded between the PIFAs with the L_r = 9 nH and C_r = 0.3 pF. As shown in Fig. 7(a), the addition

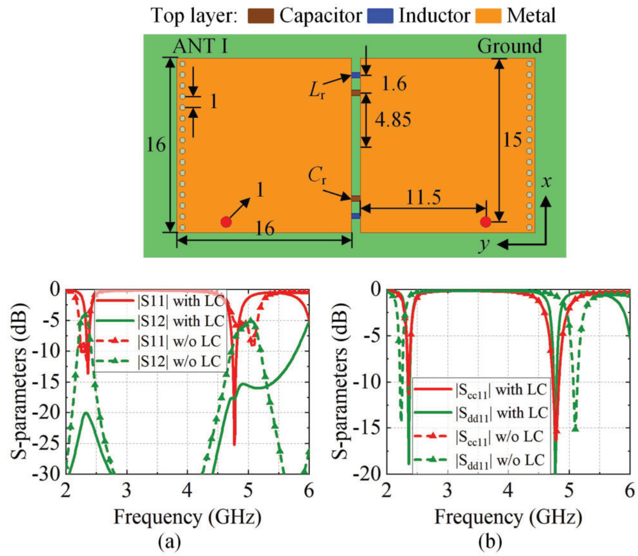

Fig. 7. Simulated (a) passive and (b) CM/DM S-parameters of Ant I with the decoupling *LC* resonator.

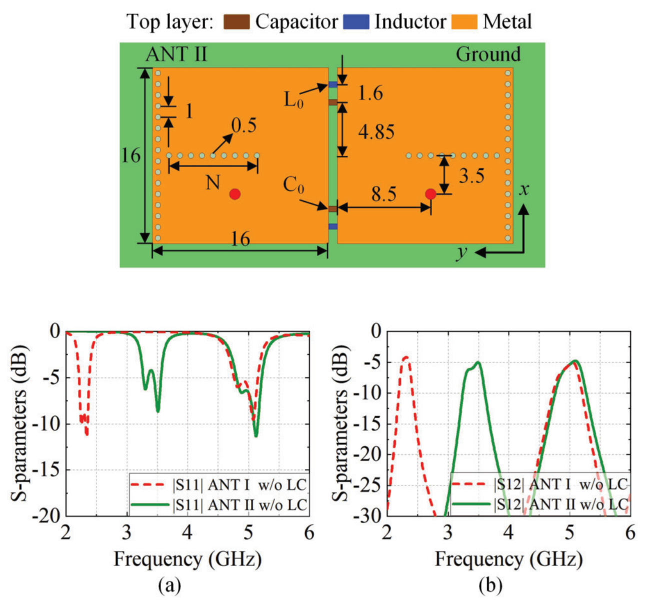

Fig. 8. Simulated (a) |S11| and (b) |S12| of Ant II with shorting pins loaded in the center line.

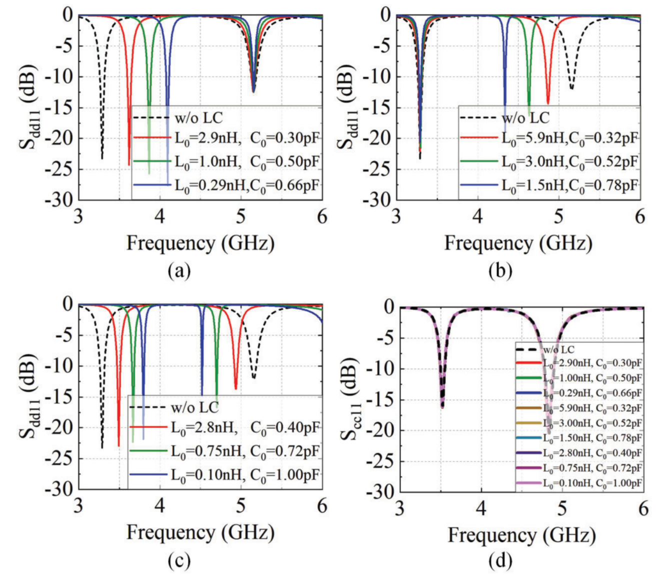

Fig. 9. Simulated DM S-parameters of Ant II with N = 9 utilizing a combination of *LC* resonators in adjustment of (a) $TM_{0,0.5}$ mode in the lower band, (b) $TM_{1,0.5}$ mode in the higher band, and (c) both the operating modes. (d) Simulated CM S-parameters with different combinations of *LC* resonators.

of the decoupling *LC* resonator significantly enhances the isolation of Ant I from 4.2 to 20.1 dB in the lower frequency band and 5.1 to 15.3 dB in the higher frequency band. Fig. 7(b) demonstrates that the introduction of the decoupling *LC* resonator independently adjusts the operating frequency of DM in both bands without affecting the operation of CM. This property simplifies the decoupling process.

III. Dual-Band Decoupling With Different Frequency Ratios

To validate the effectiveness of the proposed dual-band decoupling method for antennas with different frequency ratios, Ant II with an adjustable frequency ratio is proposed. Fig. 8 displays the configuration of Ant II. To adjust the operating frequency of the $TM_{0,0.5}$ mode in the lower frequency band, N shorting pins are loaded on the centerline of PIFAs. As shown in Fig. 2, the electric field distribution of the $TM_{1,0.5}$ mode exhibits a null along the center line, implying that the addition of shorting pins does not influence the mode. Whereas, in the $TM_{0,0.5}$ mode, the strong electric field is distributed on the centerline, and the inclusion of shorting pins increases the operating frequency of this mode. As shown in Fig. 8(a) and (b), when nine pins are applied to the PIFA, the operating frequency of the lower frequency band is increased from 2.3 to 3.4 GHz. By varying the number of shorting pins N, adjustment of the frequency ratio can be realized, demonstrating the flexibility of the design.

Fig. 9 presents the simulated CM and DM S-parameters with different combinations of *LC* resonators. As shown in Fig. 9(a)–(c), by altering the resonant frequency and quality factor Q of the *LC* resonator, independent adjustment or simultaneous co-adjustment of DMs of $TM_{0,0.5}$ and $TM_{1,0.5}$ modes can be achieved. The process of adjusting the DM modes in both frequency bands is intuitive. Meanwhile, as demonstrated in Fig. 9(d), modifications to the *LC* resonator have no effect on the CM operation in the two bands. Taking advantage of this feature, the operating frequencies of CM/DM mode can be aligned, enabling dual-band decoupling in a simple manner.

The decoupling performance of the two PIFAs at various frequency ratios is presented in Fig. 10. By varying the number of shorting pins N, the operating frequency of the lower frequency band can be increased while maintaining the frequency of the higher frequency band constant. When N increases from 6 to 12 in an increment of 3, the frequency ratio between the two bands decreases from 1.7 to 1.1. In the decoupling design process, we first tune the position of the feeding probes to ensure that the CMs on both frequency bands have good impedance matching. Subsequently, by changing the characteristic parameters of the *LC* resonator, the decoupling of different frequency ratios can be achieved. As the frequency ratio decreases, the required decoupling inductor L_r decreases, and the decoupling capacitor C_r increases, which means a

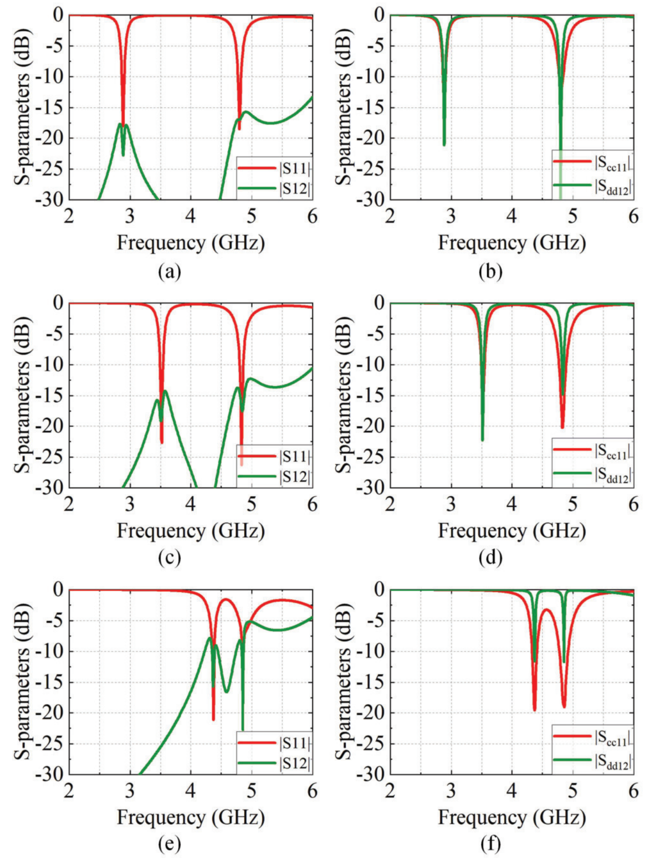

Fig. 10. Simulated (a) passive S-parameters and (b) CM/DM S-parameters of Ant II with N = 6, L_r = 4.8 nH, C_r = 0.37 pF. Simulated (c) passive S-parameters and (d) CM/DM S-parameters of Ant II with N = 9, L_r = 2.0 nH, C_r = 0.50 pF. Simulated (e) passive S-parameters and (f) CM/DM S-parameters of Ant II with N = 12, L_r = 0 nH, C_r = 0.90 pF.

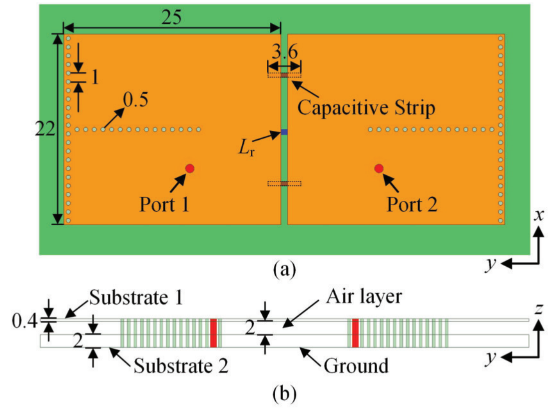

Fig. 11. Configuration of the proposed antenna. (a) Top view. (b) Side view.

higher Q-factor of the LC resonator. As shown in Fig. 9(a)–(c), as the Q-factor of the LC resonator increases, the operating frequency of the DM is adjusted more significantly. However, loading the antennas with a high-Q LC resonator also leads to a narrower bandwidth on DMs. This phenomenon is mainly attributed to the more pronounced frequency-dependent impedance characteristics of the LC resonator with higher Q-factors. Although the bandwidths of DMs are constrained, LC resonators with high Q-factor allow for substantial tuning of the resonant frequency of DMs. Consequently, the peak isolation is not significantly compromised with the use of high-Q LC resonators.

IV. Simplified Design of Dual-Band Decoupling With Step-by-Step Adjustment of Two Operating Bands

To facilitate the independent adjustment of decoupling for the two bands of the antenna, as displayed in Fig. 11, the placement of the LC resonator components is optimized. As illustrated in Fig. 2, the electric field distribution exhibits distinct null points between the $TM_{0,0.5}$ and $TM_{1,0.5}$ modes. When a lumped component is positioned at the null point of a particular mode, it exerts negligible influence on the operation of the mode. In the proposed design shown in Fig. 11, the inductive component of the decoupled resonator is centrally loaded, while the capacitive component is positioned near the edge of the antenna. This configuration enables decoupling adjustments for each frequency band independently, streamlining the tuning process.

The structure of the proposed antenna, as depicted in Fig. 11, comprises three layers: the upper FR-4 dielectric substrate, the middle air layer, and the lower FR-4 dielectric substrate. The substrate configuration is widely utilized in mobile terminal designs. Due to the small capacitance values required in this design, which exceed the precision of standard commercial components, the multilayer dielectric structure provides a convenient means of achieving high-accuracy capacitance. Specifically, two metal strips are incorporated on the lower surface of substrate 1, creating a strong electric field distribution between the strips and the patch. By varying the length of the strips, different equivalent capacitance values can be achieved in the gaps between the two PIFAs. Moreover, the introduction of the air layer significantly enhances the antenna efficiency by reducing the loss of FR-4, further improving the overall performance of the structure.

The proposed decoupling scheme and the corresponding S-parameters are presented in Figs. 12 and 13. The decoupling process is implemented in three steps. In the first step, the operating frequencies of the CMs in the two bands are adjusted by adjusting the antenna dimensions and the number of shorting pins. Subsequently, the feeding position is tuned to ensure that the two CMs are well-matched within the desired frequency bands, as depicted in Fig. 13(c). In the second step, two capacitors are introduced to lower the operating frequency of the DM for the $TM_{1,0.5}$ mode in the higher frequency band. As shown in Fig. 13(b) and (d), by incorporating the capacitors, the operating frequency of the DM for the $TM_{1,0.5}$ is reduced to the desired band, and the isolation is enhanced. Finally, an inductor is placed at the center of the PIFAs. This addition increases the operating frequency of the DM for the $TM_{0,0.5}$ mode to the desired lower frequency band, effectively eliminating the mutual coupling in the lower band. Since the inductor is positioned at the electric field null of the $TM_{1,0.5}$ mode, the adjustment of the mutual coupling in the lower band can be performed separately. The revised LC resonator arrangement simplifies the decoupling process for the dual-band antenna pair, reducing the need for iterative tuning and optimization while improving overall design efficiency. The introduced lumped component in each step is only required to tune the resonant frequency of one mode to the desired band, avoiding multiobjective optimization. The design guidelines are summarized as follows.

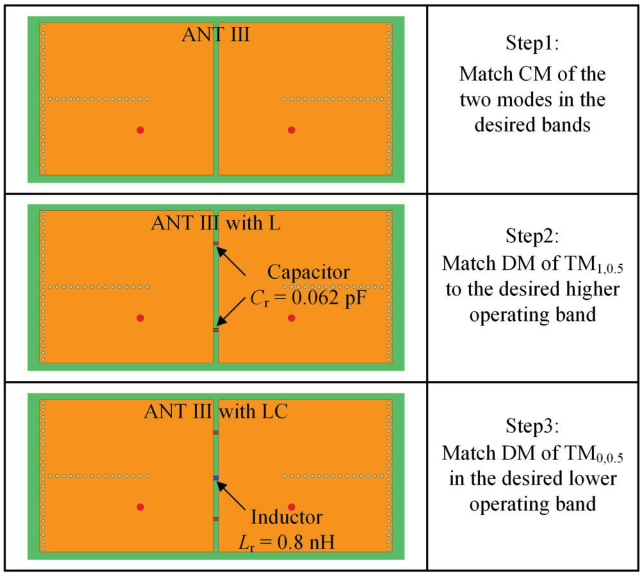

Fig. 12. Design process of the decoupling design with easy adjustment of the two bands without repeated iteration.

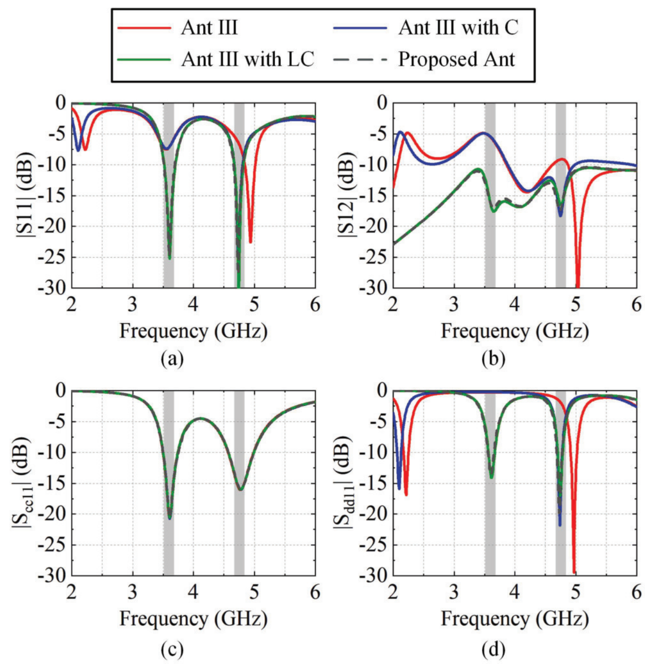

Fig. 13. Simulated S-parameters of Ant III with different decoupling structures in the design process. (a) |S11|. (b) |S12|. (c) $|S_{cc11}|$. (d) $|S_{dd11}|$.

1) Adjusting the feeding position to achieve impedance matching for both CMs and DMs in the two frequency bands.
2) Introduce capacitors to lower the resonant frequency of DM of the $TM_{1,0.5}$ to align with the resonant frequency of CM, thereby achieving decoupling of the higher frequency band.
3) Introduce an inductor at the center of the antenna to raise the resonant frequency of DM of the $TM_{0,0.5}$ to align with the resonant frequency of CM, thereby achieving decoupling of the lower frequency band.

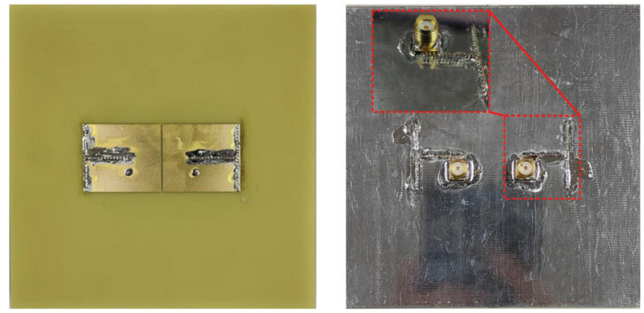

(a) (b)

Fig. 14. Configuration of the fabricated prototype. (a) Top view. (b) Bottom view.

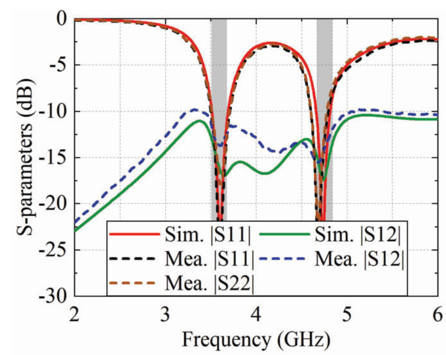

Fig. 15. Simulated and measured S-parameters of the proposed antenna.

Given the requirement for a small capacitance value, two capacitive strips are employed instead of lumped capacitors in the proposed antenna. As illustrated in Fig. 13, the S-parameters of the proposed antenna are consistent with those of Ant III with *LC*. The capacitor strips are equivalent to two 0.062 pF capacitors. In the decoupling process, the inclusion of lumped components has no effect on the CMs but shifts the operating frequency of the two DMs. By precisely tuning the operating frequency of the DMs to match those of the CMs, the impedance difference between the CMs and DMs is minimized. This alignment allows for simultaneous impedance matching and decoupling across the two operating bands.

V. Fabrication of Design Example and Measurement

To validate the decoupling scheme, the proposed antenna is fabricated and measured. Fig. 14 depicts the fabricated prototype of the proposed antenna. The two substrates of the antenna are held together by metal rods with a diameter of 0.5 mm. The metal rods are soldered to the top and bottom substrates, which act as the shorting pins of the PIFAs. A lumped inductor with a package of 0402 is employed as the decoupling inductor.

The simulated and measured S-parameters of the proposed antenna are presented in Fig. 15. The proposed antennas cover the frequency bands of 3.50~3.71 GHz and 4.61~4.79 GHz. The isolation of the lower frequency band and the higher frequency band is improved from 5 and 9 dB to 14 and 15 dB, respectively. Effective decoupling is achieved across both frequency bands. The measured results agree with the simulated results. The simulated and measured radiation patterns of the proposed antenna at both bands are depicted

TABLE I
COMPARISON AMONG THE DECOUPLING DESIGNS OF DUAL-BAND ANTENNAS

Reference	Decoupling scheme	Structure Complexity	Size (λ_0^3)	Frequency ratio	Initial isolation (dB)	Decoupling isolation (dB)	Bandwidth	Substrate
[23]	Metasurface	Complex	0.83×0.50×0.14	1.3	LB: 8; HB: 14	LB: 23; HB: 28	LB: 2.9% HB: 28.6%	F4B (ε_r=4.4)
[28]	Decoupling resonator	Complex	0.51×0.18×0.08	2.1	LB: 8; HB: 14	LB: 23; HB: 26	LB: 5.7% HB: 22.4%	AIR (ε_r=1.0)
[29]	Decoupling resonator	Complex	0.78×0.55×0.02	1.2	LB: 12; HB: 9	LB: 28; HB: 27	LB: 2.0% HB: 2.4%	FR-4 (ε_r=4.4)
[36]	DGS+ Metasurface	Complex	0.64×0.27×0.22	1.1	LB: 6; HB: 10	LB: 43; HB: 28	LB: 1.5% HB: 2.1%	F4B (ε_r=2.65)
[40]	Decoupling inductor	Simple	/	1.4	LB: 5; HB: 7	LB: 12; HB: 15	LB: 5.8% HB: 4.1%	FR-4 (ε_r=4.4)
This work	Decoupling resonator	Simple	0.59×0.25×0.05	2.0~1.1	LB: 5; HB: 9	LB: 14; HB: 15	LB: 5.8% HB: 3.8%	FR-4 (ε_r=4.4)

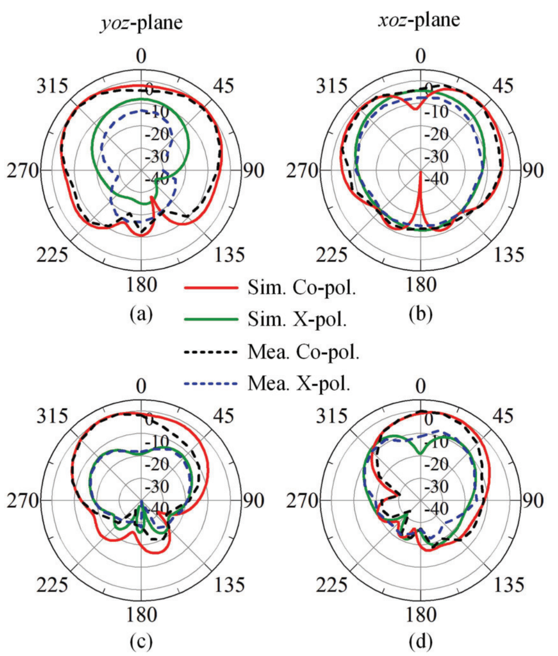

Fig. 16. Simulated and measured normalized radiation pattern of port 1 of the proposed antenna. (a) *yoz*-plane at 3.6 GHz. (b) *xoz*-plane at 3.6 GHz. (c) *yoz*-plane at 4.75 GHz. (d) *xoz*-plane at 4.75 GHz.

in Fig. 16. For single-port excitation, the radiation pattern tilts slightly due to the residual current on the adjacent parasitic element. Peak gains of 5.17 and 6.70 dBi are realized at 3.6 and 4.75 GHz, respectively.

To validate the radiation performance of the proposed antenna, measurements were performed in a multiprobe anechoic chamber, RayZone 1800. With 12 antenna probes arranged in a circular formation, the system enables measurement of 3-D radiation pattern measurements by rotating the antenna under test in the horizontal plane. Fig. 17 presents the simulated and measured efficiencies and envelope correlation coefficients (ECCs). The measured efficiencies of the proposed antennas range from 71.4% to 85.5% in the lower frequency band and from 60.2% to 71.1% in the higher frequency band. Due to the fabrication errors, the measured efficiency peaks in both bands show a certain frequency shift due to the shift of the resonant point. In general, the measured results are in good agreement with the simulated results. To evaluate the

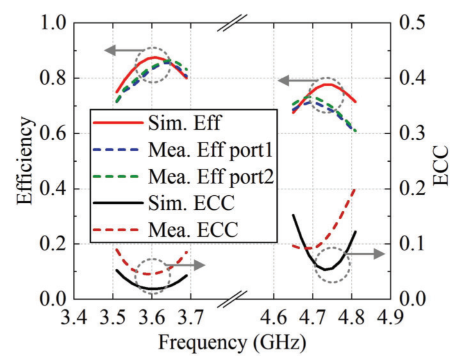

Fig. 17. Simulated and measured efficiency and ECC of the proposed antenna.

diversity performance of the proposed antennas, the ECCs are calculated based on the far-field results. The measured ECCs are below 0.09 in the lower band and below 0.20 in the upper band, which implies good diversity performance. The measured gains of port 1 in the two bands reach 4.7 and 7.0 dBi, respectively, and the measured gains of port 2 in the two bands reach 4.9 and 7.2 dBi, respectively.

VI. COMPARISON

To demonstrate the superiority of the proposed scheme, a comparison with previous dual-band decoupling designs is presented in Table I. In [11], [28], [29], and [36], although good decoupling performance is achieved, the decoupling structure and the design process are complex, which require numerous iterative optimizations. The DGS, metasurface, and decoupling resonators occupy extra spaces. When the frequency ratio is decreased, the dual-band decoupled structures interfere with each other, which complicates the design process. A simple decoupling structure utilizing a single inductor is proposed in [40] with a similar decoupling bandwidth and isolation in both bands. However, the single inductor can only be applied to dual-band antennas with a fixed frequency ratio. In our work, we present a method for analyzing coupling characteristics, enabling a straightforward identification of the decoupling lumped components required in each frequency band. Lumped *LC* resonators are applied to the decoupling of dual-band antennas with a simple structure. By observing the operating frequency of the differential mode in the two bands, the value of *LC* can be easily determined. Our proposed scheme can be applied to antennas with a small frequency ratio of 1.1. The design process has clear and simple design guidelines while providing good decoupling performance.

VII. Conclusion

In this article, a dual-band decoupling scheme is proposed with a simple structure, flexible frequency ratio, and compact size. PIFA has opposite coupling characteristics in different operating modes. While *LC* resonators also exhibit opposite impedance characteristics at different frequencies. Taking advantage of this characteristic, we propose to use *LC* resonators in the decoupling of the dual-mode PIFAs operating in two frequency bands. By changing the operating frequency and Q value of the *LC* resonator, decoupling of dual-band PIFAs with different frequency ratios can be achieved. By adjusting the position of the *LC* components, the decoupling of the two bands can be realized in steps. The decoupling is simple to implement without numerous optimization iterations. The proposed scheme has potential in the design and application of MIMO systems.

References

[1] Y. Zhang and Y. Li, "Wideband microstrip antenna in small volume without using fundamental mode," *Electromagn. Sci.*, vol. 1, no. 2, pp. 1–6, Jun. 2023.

[2] Y. Zhang, Y. Li, W. Zhang, Z. Zhang, and Z. Feng, "Omnidirectional antenna diversity system for high-speed onboard communication," *Engineering*, vol. 11, pp. 72–79, Apr. 2022.

[3] M. Chen, L. Chang, and A. Zhang, "Heat-dissipating mobile antenna: A novel mobile antenna concept with extremely small clearance and integrated heat-dissipating function," *IEEE Trans. Antennas Propag.*, vol. 72, no. 10, pp. 7480–7492, Oct. 2024.

[4] S. Gao, L. Chang, S. Gao, and A. Zhang, "Distributed mobile antennas: A novel miniaturized wideband antenna strategy to maximize the use of thse fragmented spaces of the mobile terminals," *IEEE Trans. Antennas Propag.*, vol. 72, no. 9, pp. 7017–7029, Sep. 2024.

[5] M. A. Jensen and J. W. Wallace, "A review of antennas and propagation for MIMO wireless communications," *IEEE Trans. Antennas Propag.*, vol. 52, no. 11, pp. 2810–2824, Nov. 2004.

[6] E. Rajo-Iglesias, Ó. Quevedo-Teruel, and L. Inclan-Sanchez, "Mutual coupling reduction in patch antenna arrays by using a planar EBG structure and a multilayer dielectric substrate," *IEEE Trans. Antennas Propag.*, vol. 56, no. 6, pp. 1648–1655, Jun. 2008.

[7] B. Qian, X. Chen, L. Zhao, J. Chen, and A. A. Kishk, "Reduced cross-polarization and backside radiations for rectangular microstrip antennas using defected ground structure combined with decoupling structure," *IEEE Antennas Wireless Propag. Lett.*, vol. 22, pp. 517–521, 2023.

[8] Y. Wang and Z. Du, "A wideband printed dual-antenna system with a novel neutralization line for mobile terminals," *IEEE Antennas Wireless Propag. Lett.*, vol. 12, pp. 1428–1431, 2013.

[9] Y. Wang and Z. Du, "A wideband printed dual-antenna with three neutralization lines for mobile terminals," *IEEE Trans. Antennas Propag.*, vol. 62, no. 3, pp. 1495–1500, Mar. 2014.

[10] M. Li, L. Jiang, and K. L. Yeung, "A general and systematic method to design neutralization lines for isolation enhancement in MIMO antenna arrays," *IEEE Trans. Veh. Technol.*, vol. 69, no. 6, pp. 6242–6253, Jun. 2020.

[11] F. Liu, J. Guo, L. Zhao, G.-L. Huang, Y. Li, and Y. Yin, "Dual-band metasurface-based decoupling method for two closely packed dual-band antennas," *IEEE Trans. Antennas Propag.*, vol. 68, no. 1, pp. 552–557, Jan. 2020.

[12] G. Zhao, T. Liu, J. Jiang, L. Zhao, G.-L. Huang, and W. Lin, "Polarization selective partial reflective decoupling layers for mutual coupling reduction of two closely spaced dual-polarized antennas," *IEEE Trans. Antennas Propag.*, vol. 70, no. 11, pp. 11205–11210, Nov. 2022.

[13] T. Pei, L. Zhu, J. Wang, and W. Wu, "A low-profile decoupling structure for mutual coupling suppression in MIMO patch antenna," *IEEE Trans. Antennas Propag.*, vol. 69, no. 10, pp. 6145–6153, Oct. 2021.

[14] S.-W. Su, C.-T. Lee, and Y.-W. Hsiao, "Compact two-inverted-F-antenna system with highly integrated π-shaped decoupling structure," *IEEE Trans. Antennas Propag.*, vol. 67, no. 9, pp. 6182–6186, Sep. 2019.

[15] M. Chen, L. Chang, and A. Zhang, "Wideband antenna pairs consisting of E-/M-coupling frame monopoles and M-/E-coupling back cover patches for mobile terminal applications," *IEEE Trans. Antennas Propag.*, vol. 72, no. 2, pp. 1308–1318, Feb. 2024.

[16] L. Sun, Y. Li, Z. Zhang, and H. Wang, "Antenna decoupling by common and differential modes cancellation," *IEEE Trans. Antennas Propag.*, vol. 69, no. 2, pp. 672–682, Feb. 2021.

[17] L. Sun, Y. Li, and Z. Zhang, "Decoupling between extremely closely spaced patch antennas by mode cancellation method," *IEEE Trans. Antennas Propag.*, vol. 69, no. 6, pp. 3074–3083, Jun. 2021.

[18] J. Hu, W. Zhang, Y. Li, and Z. Zhang, "Compact co-polarized PIFAs for full-duplex application based on CM/DM cancellation theory," *IEEE Trans. Antennas Propag.*, vol. 69, no. 11, pp. 7103–7110, Nov. 2021.

[19] Z. Cao, L. Chang, Y. Li, K. Wei, and Z. Zhang, "Decoupling of axial symmetric three antennas based on active impedance matching," *IEEE Trans. Antennas Propag.*, vol. 72, pp. 6919–6929, 2024.

[20] S. Soltani, P. Lotfi, and R. D. Murch, "A dual-band multiport MIMO slot antenna for WLAN applications," *IEEE Antennas Wireless Propag. Lett.*, vol. 16, pp. 529–532, 2017.

[21] S. Nandi and A. Mohan, "A compact dual-band MIMO slot antenna for WLAN applications," *IEEE Antennas Wireless Propag. Lett.*, vol. 16, pp. 2457–2460, 2017.

[22] L. Guo, Y. Wang, Z. Du, Y. Gao, and D. Shi, "A compact uniplanar printed dual-antenna operating at the 2.4/5.2/5.8 GHz WLAN bands for laptop computers," *IEEE Antennas Wireless Propag. Lett.*, vol. 13, pp. 229–232, 2014.

[23] W. Wang, Y. Wu, W. Wang, and Y. Yang, "Isolation enhancement in dual-band monopole antenna for 5G applications," *IEEE Trans. Circuits Syst. II, Exp. Briefs*, vol. 68, no. 6, pp. 1867–1871, Jun. 2021.

[24] Q. Zheng, J. Wang, P. PourMohammadi, and X. Pang, "Dual-band metasurface-based closely packed antennas by controlling surface wave propagation," *IEEE Antennas Wireless Propag. Lett.*, vol. 23, pp. 1633–1637, 2024.

[25] X. Ling and R. Li, "A novel dual-band MIMO antenna array with low mutual coupling for portable wireless devices," *IEEE Antennas Wireless Propag. Lett.*, vol. 10, pp. 1039–1042, 2011.

[26] L. Wen, M. Zhang, W. Hu, Q. Yang, and W. Xiao, "Coupling cancellation using coupling stubs for MIMO array applications," *IEEE Antennas Wireless Propag. Lett.*, vol. 23, pp. 204–208, 2024.

[27] W. Zhang, Y. Li, K. Wei, and Z. Zhang, "A dual-band MIMO antenna system for 2.4/5 GHz WLAN applications," *IEEE Trans. Antennas Propag.*, vol. 71, no. 7, pp. 5749–5758, Jul. 2023.

[28] W. Zhang, Y. Li, K. Wei, and Z. Zhang, "Dual-band decoupling for two back-to-back PIFAs," *IEEE Trans. Antennas Propag.*, vol. 71, no. 3, pp. 2802–2807, Mar. 2023.

[29] B. L. Dhevi, K. S. Vishvaksenan, and K. Rajakani, "Isolation enhancement in dual-band microstrip antenna array using asymmetric loop resonator," *IEEE Antennas Wireless Propag. Lett.*, vol. 17, pp. 238–241, 2018.

[30] X. Shen et al., "Decoupling of two strongly coupled dual-band antennas with reactively loaded dummy element array," *IEEE Access*, vol. 7, pp. 154672–154682, 2019.

[31] L. Cui, J. Guo, Y. Liu, and C.-Y.-D. Sim, "An 8-element dual-band MIMO antenna with decoupling stub for 5G smartphone applications," *IEEE Antennas Wireless Propag. Lett.*, vol. 18, pp. 2095–2099, 2019.

[32] J.-H. Xun, L.-F. Shi, W.-R. Liu, G.-X. Liu, and S. Chen, "Compact dual-band decoupling structure for improving mutual coupling of closely placed PIFAs," *IEEE Antennas Wireless Propag. Lett.*, vol. 16, pp. 1985–1989, 2017.

[33] J. Yin, Y. Jia, S. Yang, and H. Zhai, "Design of a composite decoupling structure for dual-band dual-polarized base station array," *IEEE Antennas Wireless Propag. Lett.*, vol. 21, pp. 1408–1412, 2022.

[34] J. Zhu, J. Wang, and X. Fu, "Design of an effective low profile decoupling structure for adjacent dual-band patch antennas," in *Proc. Cross Strait Radio Sci. Wireless Technol. Conf. (CSRSWTC)*, Fuzhou, China, Dec. 2020, pp. 1–3.

[35] J. Deng, J. Li, L. Zhao, and L. Guo, "A dual-band inverted-F MIMO antenna with enhanced isolation for WLAN applications," *IEEE Antennas Wireless Propag. Lett.*, vol. 16, pp. 2270–2273, 2017.

[36] Z. Niu, H. Zhang, Q. Chen, and T. Zhong, "Isolation enhancement in closely coupled dual-band MIMO patch antennas," *IEEE Antennas Wireless Propag. Lett.*, vol. 18, pp. 1686–1690, 2019.

[37] J. Sui, Y.-F. Cheng, X. Fang, D. Li, X. Zhu, and X. Yuan, "A dual-band decoupling technique for MIMO antenna systems using composite capacitor circuits," *IEEE Trans. Circuits Syst. II, Exp. Briefs*, vol. 71, no. 1, pp. 116–120, Jan. 2024.

[38] L. Zhao, L. K. Yeung, and K.-L. Wu, "A coupled resonator decoupling network for two-element compact antenna arrays in mobile terminals," *IEEE Trans. Antennas Propag.*, vol. 62, no. 5, pp. 2767–2776, May 2014.

[39] J. Sui and K.-L. Wu, "A general T-stub circuit for decoupling of two dual-band antennas," *IEEE Trans. Microw. Theory Techn.*, vol. 65, no. 6, pp. 2111–2121, Jun. 2017.

[40] C. Deng, X. Cao, D. Li, and W. Yu, "Compact dual-band MIMO antenna with shared decoupling structure for 5G mobile terminals," *IEEE Antennas Wireless Propag. Lett.*, vol. 22, no. 6, pp. 1281–1285, Jun. 2023.

[41] D. Chen, Q. Xue, W. Yang, K.-S. Chin, H. Jin, and W. Che, "A compact wideband low-profile metasurface antenna loaded with patch-via-wall structure," *IEEE Antennas Wireless Propag. Lett.*, vol. 22, pp. 179–183, 2023.

[42] L. Chang, G. Zhang, and H. Wang, "Triple-band microstrip patch antenna and its four-antenna module based on half-mode patch for 5G 4×4 MIMO operation," *IEEE Trans. Antennas Propag.*, vol. 70, no. 1, pp. 67–74, Jan. 2022.

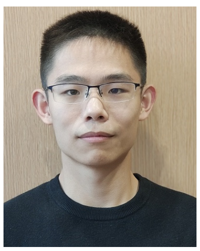

Zhongyao Cao received the B.S. degree from the University of Electronic Science and Technology of China, Chengdu, China, in 2020. He is currently pursuing the Ph.D. degree in electrical engineering with Tsinghua University, Beijing, China.

His current research interests include reconfigurable antennas, beam scanning arrays, and reflectarray antennas.

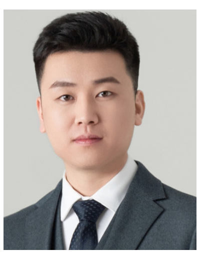

Le Chang (Senior Member, IEEE) received the B.S. degree in electronics and information engineering from Xidian University, Xi'an, China, in 2012, and the Ph.D. degree in electrical engineering from Tsinghua University, Beijing, China, in 2017.

In July 2017, he joined Huawei Technology Ltd., Beijing, as a Senior Antenna Engineer. Since 2021, he has been with Xi'an Jiaotong University, Xi'an, where he is currently an Associate Professor. He has authored or co-authored 45 journal articles. His current research interests include mobile antennas and mmW/THz antennas.

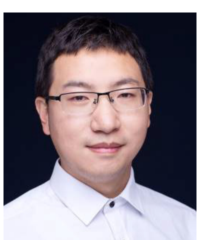

Yue Li (Senior Member, IEEE) received the B.S. degree in telecommunication engineering from Zhejiang University, Hangzhou, Zhejiang, China, in 2007, and the Ph.D. degree in electronic engineering from Tsinghua University, Beijing, China, in 2012.

In June 2012, he was a Post-Doctoral Fellow with the Department of Electronic Engineering, Tsinghua University. In December 2013, he was a Research Scholar with the Department of Electrical and Systems Engineering, University of Pennsylvania, Philadelphia, PA, USA. He was also a Visiting Scholar with the Institute for Infocomm Research (I2R), A*STAR, Singapore, in 2010, and Hawaii Center of Advanced Communication (HCAC), University of Hawaii at Manoa, Honolulu, HI, USA, in 2012. Since January 2016, he has been with Tsinghua University, where he is currently an Assistant Professor and an Associate Professor with the Department of Electronic Engineering. He has authored and co-authored over 250 journal articles and 50 international conference papers. He holds 26 granted Chinese patents. His current research interests include metamaterials, plasmonics, electromagnetics, nanocircuits, mobile and handset antennas, MIMO and diversity antennas, and millimeter-wave antennas and arrays.

Dr. Li was a recipient of the Issac Koga Gold Medal from URSI General Assembly. He served as an Associate Editor for IEEE TRANSACTIONS ON ANTENNAS AND PROPAGATION and IEEE ANTENNAS AND WIRELESS PROPAGATION LETTERS from 2017 to 2024. He is also serving as an Associate Editor for *Microwave and Optical Technology Letters* and *Computer Applications in Engineering Education*.

Kunpeng Wei (Senior Member, IEEE) received the B.S. degree in electronic and information engineering from the Huazhong University of Science and Technology, Wuhan, China, in 2008, and the Ph.D. degree in electrical engineering from Tsinghua University, Beijing, China, in 2013.

In 2012, he was a Visiting Scholar with the School of Electrical and Computer Engineering, Georgia Institute of Technology, Atlanta, GA, USA. From July 2013 to December 2015, he was employed with the Radar Research Institute of Chinese Air Force Research Laboratory, Wuhan, conducting research in the areas of phased-array antenna design and radar system design. He joined Consume Business Group of Huawei Inc., Shenzhen, China, in 2016, where he had been an Antenna Specialist and the Director of Xi'an Antenna Team. Since 2021, he joined Honor Device Company Ltd., Shenzhen, when this company split from Huawei and he was the Director of Honor Antenna Team. After leaving Honor, he joined Xiaomi Corporation, Beijing, in 2023. He is currently the Chief Antenna Expert and the Head of the Antenna Technology Team. He is also an Adjunct Professor with the School of Electronics and Information Engineering, Shenzhen University, Shenzhen. He leads a large group of antenna experts and engineers and takes full responsibility for the research of antenna technologies to guarantee the market success of all Xiaomi's products, ranging from smartphones, electric cars, tablets, and other IOT devices. He has authored over 60 articles on consumer electronics antenna design. He holds over 100 granted U.S./EU/JP/CN patents and has more than 20 patent applications pending. His current research interests include MIMO antenna technology, satellite communication technology, 5.5G/millimeter wave technology, UWB wireless technology, and meta-antennas for "Human x Car x Home" smart ecosystems.

Dr. Wei is an IET Fellow. He was a recipient of the Principal Scholarship of Tsinghua University in 2012, Huawei Individual Gold Medal Award in 2018, Huawei Team Gold Medal Award in 2017, and the Honor Team Gold Medal Award in 2021, respectively. He is serving as an Associate Editor for *IET Electronics Letters* since October 2021 and IEEE OPEN JOURNAL OF ANTENNAS AND PROPAGATION since October 2023. He is also a special-level external expert of China Academy of Information and Communications Technology.

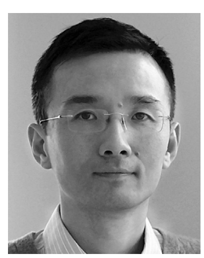

Zhijun Zhang (Fellow, IEEE) received the B.S. and M.S. degrees from the University of Electronic Science and Technology of China, Chengdu, China, in 1992 and 1995, respectively, and the Ph.D. degree from Tsinghua University, Beijing, China, in 1999.

In 1999, he was a Post-Doctoral Fellow with the Department of Electrical Engineering, University of Utah, Salt Lake City, UT, USA, where he was appointed a Research Assistant Professor in 2001. In May 2002, he was an Assistant Researcher with the University of Hawaii at Manoa, Honolulu, HI, USA. In November 2002, he joined Amphenol T&M Antennas, Vernon Hills, IL, USA, as a Senior Staff Antenna Development Engineer and was then promoted to the position of Antenna Engineer Manager. In 2004, he joined Nokia Inc., San Diego, CA, USA, as a Senior Antenna Design Engineer. In 2006, he joined Apple Inc., Cupertino, CA, USA, as a Senior Antenna Design Engineer, and was then promoted to the position of the Principal Antenna Engineer. Since August 2007, he has been with Tsinghua University, where he is a Professor with the Department of Electronic Engineering.

Dr. Zhang is the author of *Antenna Design for Mobile Devices* (Wiley, first edition 2011, second edition 2017). He served as an Associate Editor for IEEE TRANSACTIONS ON ANTENNAS AND PROPAGATION from 2010 to 2014 and IEEE ANTENNAS AND WIRELESS PROPAGATION LETTERS from 2009 to 2015.